Chapter 4

OPLAH ablation leads to accumulation of 5-oxoproline, oxidative stress, fibrosis and elevated fillings pressures in a murine model for heart failure with a preserved ejection fraction

Atze van der Pol[1], Andres Gil[2], Jasper Tromp[1,3], Herman H.W. Silljé[1], Dirk J. van Veldhuisen[1], Adriaan A. Voors[1], Elke S. Hoendermis[1], Niels Grote Beverborg[1], Elisabeth-Maria Schouten[1], Rudolf A. de Boer[1], Rainer Bischoff[2], Peter van der Meer[1]

[1]Department of Cardiology, University Medical Center Groningen, University of Groningen
[2]Department of Pharmacy, Analytical Biochemistry, University of Groningen
[3]National Heart Centre Singapore

Under review at Cardiovascular Research

Abstract

Aims: The prevalence of heart failure with a preserved ejection fraction (HFpEF) is increasing, but therapeutic options are limited. Oxidative stress is suggested to play an important role in the pathophysiology of HFpEF. However, whether oxidative stress is a bystander due to comorbidities or causative in itself remains unknown. Recent results have shown that depletion of 5-oxoprolinase (OPLAH) leads to 5-oxoproline accumulation, which is an important mediator of oxidative stress in the heart. We hypothesize that oxidative stress induced by elevated levels of 5-oxoproline leads to the onset of a murine HFpEF-like phenotype.

Methods and Results: Oplah full body knock-out (KO) mice had higher 5-oxoproline levels coupled to increased oxidative stress. Compared to wild-type littermates (WT), KO mice had increased cardiac and renal fibrosis with concurrent elevated left ventricular filling pressures, impaired LV relaxation, yet a normal left ventricular ejection fraction (LVEF). Following the induction of cardiac ischemia/reperfusion (IR) injury, 52.4% of the KO mice died compared to, only 15.4% of the WT mice ($p<0.03$). Furthermore, KO mice showed a significantly increased atrial, ventricular, kidney, and liver weights compared to WT mice ($P<0.05$ for all). Cardiac and renal fibrosis were more pronounced following cardiac IR injury in the KO mice and these mice developed proteinuria post IR injury. To further address the link between 5-oxoproline and HFpEF, 5-oxoproline was measured in the plasma of HFpEF patients. Compared to healthy controls (3.8 ± 0.6 μM), 5-oxoproline levels were significantly elevated in HFpEF patients (6.8 ± 1.9 μM, $P<0.0001$). Furthermore, levels of 5-oxoproline were independently associated with more concentric remodeling on echocardiography.

Conclusions: Oxidative stress induced by 5-oxoproline results in a murine phenotype reminiscent of the clinical manifestation of HFpEF without the need for surgical or pharmacological interference. Better understanding the role of oxidative stress in HFpEF may potentially lead to novel therapeutic options.

Introduction:

Heart failure (HF) is associated with high mortality and morbidity (1). While treatment possibilities for patients with HF and a reduced ejection fraction (HFrEF) have considerably improved outcomes, this has not been the case for HF patients with a preserved ejection fraction (HFpEF) (2). The incidence of HFpEF has increased rapidly during the past decades and is becoming the dominant form of HF (2). Typical features of HFpEF include elevated LV filling pressures, impaired relaxation and structural abnormalities (i.e. left ventricular concentric remodeling). Unfortunately, the underlying pathophysiology of HFpEF remains poorly understood. To increase our understanding of the pathophysiology of HFpEF, several animal models have been developed that recapitulate some, but not all the characteristics described in HFpEF patients (3,4). As a result these animal models are limited in their use in developing therapeutic strategies specifically targeting HFpEF. Therefore, it is essential to unravel the underlying cardiac pathophysiology leading to the onset of HFpEF, by developing novel animal models, which could lead to therapies directed towards HFpEF (4).

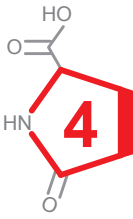

In recent years it has been suggested that oxidative stress, resulting from an increased systemic proinflammatory state, plays a role in the onset and progression of HFpEF (5). Oxidative stress is defined as an imbalance between the production of reactive oxygen species (ROS) and the endogenous antioxidant defense mechanisms (the so called “redox state”). Under physiological conditions, small quantities of ROS are produced intracellularly, which function in cell signaling, and can be readily reduced by the antioxidant defense system. However under pathophysiological conditions, the production of ROS exceeds the buffering capacity of the antioxidant defense system, resulting in cell damage and death. The major source of antioxidants in mammalian cells are glutathione (GSH), which is formed by the γ-Glutamyl cycle and thioredoxin (Trx) (6–8). Trx are small redox proteins that exert its antioxidant function primarily through peroxiredoxins (Prx), which utilizes Trx to reduce peroxides (i.e. H_2O_2). This reaction results in the formation of oxidized Trx, which can then be recycles by thioredoxin reductase (TrxR). Similarly, GSH is utilized by GSH peroxidase (GPx) to reduce H_2O_2, producing oxidized GSH (GSSG) in the process. GSSG is then recycled by GSH reductase (GR) (9). Recent studies have established an important role of the Trx antioxidant system in HF (10,11). GSH has also been implicated in cardiovascular diseases, however, only recently have the enzymes of the GSH synthesis and salvage pathways been implicated in HF (12–18).

One such enzyme is 5-oxoprolinase (OPLAH), that is responsible for converting 5-oxoproline, a degradation product of glutathione, into glutamate (6,19). 5-Oxoproline

has been shown to induce oxidative stress in rat brain tissue, rat cardiomyocytes, and human embryonic derived cardiomyocytes (16,20,21). Furthermore, OPLAH expression is reduced in both rodent models of HFrEF and in the clinical setting (16,22). This reduction of OPLAH expression is coupled to an increase in circulating 5-oxoproline, which is associated with a poor outcome in patients with HF (16). In a murine model for myocardial infarction, it was observed that OPLAH has a cardio-protective effect by reducing 5-oxoproline, oxidative stress, and improving cardiac function (16). These findings demonstrate that OPLAH and 5-oxoproline are highly involved in oxidative stress and HF, and could suggest a novel therapeutic target for HF. Based on these observations and the recent implication of oxidative stress in the development of HFpEF, we hypothesized that OPLAH knock-out (KO) mice would develop a cardiac phenotype reminiscent of clinical HFpEF. Furthermore, we were interested in identifying whether OPLAH KO mice would be more susceptible to cardiac injury.

Methods

Generation of Oplah knock-out mice

Oplah knock-out mice, Oplah$^{tm1a(KOMP)Wtsi}$ (here after referred to as KO) mice were generated as part of the European Conditional Mouse Mutagenesis Program and Knockout Mouse Project projects and the Sanger Mouse Genetics Projects (EUCOMM/KOMP-CSD) (23). Mice were generated from embryonic stem cell clone EPD0244_4_F09 and backcrossed to C57L/6 background. Genotype analysis was performed by PCR on isolated genomic DNA as previously described (25). All animal protocols were approved by the Animal Ethical Committee of the University of Groningen (permit number: DEC6632). The animal experiments were performed conform the ARRIVE guidelines (25).

Cardiac ischemia/reperfusion injury in Oplah knock-out mice

Animal protocol was approved by the Animal Ethical Committee of the University of Groningen (permit number: DEC6632). The animal experiments were performed conform the ARRIVE guidelines. A total of 103 male mice, 37 knock-out (KO), 38 heterozygous (HET) and 28 wild-type (WT), were included in the ischemia/reperfusion (IR) study. All mice were 14-20 weeks of age and 35-40 g of body weight. The KO, HET and WT mice were randomized into two groups, the SHAM operated group and the IR group. Animals were anesthetized with isoflurane and medical oxygen, followed by the administration of 5mg/kg of carprofen. The IR group (WT n = 13, HET n = 16, and KO n = 21) underwent ligation of the left anterior descending branch (LAD) of the left coronary artery for 60 min, followed by reperfusion for 4 weeks. The ligation of the LAD was placed by the surgeon to achieve a ±30% area

at risk of the LV. The SHAM operated group (WT n = 15, HET n = 22 and KO n = 16) underwent the same procedure without induction of ischemia. The surgeon was blinded to which animal was KO, HET or WT. After 4 weeks animals were placed in the MRI followed by hemodynamic measurements and animals were sacrificed. At sacrifice, blood was collected and organs were weighed and collected for histology and molecular analysis.

Cardiac MRI measurements

Cardiac MRI was performed as described previously (16,26). Mice were anesthetized with isoflurane (2%) and imaged in a vertical 9.4-T, 89-mm bore size magnet equipped with 1500 mT/m gradients and connected to an advanced 400 MR system (Bruker Biospin) using a quadrature-driven birdcage coil with an inner diameter of 3 cm. Respiration and ECG were monitored by ECG Trigger Unit (RAPID biomedical GmBH). Heart rate was maintained between 400-600 bpm and respiration rate between 20-60 breaths per minute. ParaVison 4.0 and IntraGate software (Bruker Biospin GmH) were used for cine MR acquisition and reconstruction. After orthogonal scout imaging, short axis (oriented perpendicular to the septum) cardiac cine MR images were acquired. To cover the entire heart from apex to base, 7 slices (sham) and 8-9 slices (IR) were needed. The images were reconstructed and for all mice, dedicated, semi-automatic contour detection software (QMass, version MR 6.1.5, Medis Medical Imaging Systems) was used for the determination of the LV end-diastolic volume, LV end-systolic volume, stroke volume, and ejection fraction. The investigators were blinded to experimental settings during data analysis.

Hemodynamic measurements

Heart rate and pressures of aorta and LV were measured after 4 weeks using the Scisense Advantage PV measurement system with a PV catheter, as previously described (16). A 1.2 French electrode with 4.5 spacing (Transonic Scisense Inc) was used. Analyses were performed offline with LabChart7 software (version 7.2, ADinstruments). After hemodynamic measurements, mice were sacrificed by excision of the heart and tissues and tibia were collected. The investigators were blinded to experimental settings during data analysis.

Electrocardiography

A total of 23 mice, 18 KO and 5 WT, were utilized to perform electrocardiography (ECG) measurements. All mice were 14-20 weeks of age and 35-40 g of body weight. Animals were anesthetized with isoflurane and medical oxygen, followed by the administration of 5mg/kg of carprofen. At this point 1 min baseline ECG recording was made of each animal. For ECG measurements, subcutaneous recording electrodes were placed, one in the right armpit and the other in the left groin (Lead II). Following the baseline measurements, the electrodes were removed and a ligation of the was

placed on the LAD. After which electrodes were again placed and a 45 min ECG recording was performed. At the end of the 45 min ischemic ECG recording, the animals were terminated by excision of the heart.

Histology

For immunohistochemical analysis, hearts were fixed overnight with 10% neutral-buffered formalin at 4°C. After fixation, samples were subjected to a dehydration series, embedded in paraffin and cut into 4 µM sections. Masson trichrome straining was performed to analyze collagen deposition. To quantify fibrosis, whole ventricle slice pictures were photographed using Hamamatsu microscope, and fibrotic area was determined with Aperio's ImageScope software. Areas of fibrosis were calculated as percentages of total area of the left ventricle. To quantify the infarct size, area of infarct were calculated as percentages of total area of the left ventricle. To quantify the non-infract fibrosis, fibrosis was calculated as a percentage of the total area opposite of the infarct. For cardiomyocyte size, FITC-labeled wheat germ agglutinin (WGA) staining was performed. For quantification Fiji (27) was used, briefly five randomly selected fields from whole-stained WGA-FITC LV sections imaged ad 20x magnification were used to measure cross-sectional diameter from approximately 30 cells per mouse heart, and calculated as area. The investigators were blinded to experimental settings during data analysis.

Urine measurements

Urine from mice was collected following excision of the heart directly from the bladder. To assess the total urinary protein, urea and creatinine 25 µl of urine was diluted with 225 µl MilliQ (1:10 dilution). For determining the total protein the UV assay U/CSF Protein kit (Roche Diagnostics) was used. For urea measurements the UV assay UREA/UN kit (Roche Diagnostics) was used. For creatinine measurements the UV assay CREA plus (Roche Diagnostics) was used.

Total Antioxidant Capacity

The antioxidant capacity of tissue samples was measured by means of the Total Antioxidant Capacity Assay kit (ab65329, Abcam) per manufactures instructions. Briefly, snap frozen LV tissue was homogenized in ice-cold RIPA (50 mM Tris pH 8.0, 1% nonidet P40, 0.5% deoxycholate, 0.1% SDS, 150 mM NaCl), followed by centrifugation at 12,000 rcf for 10 min at 4°C. Supernatant was collected and assayed.

Quantitative real time PCR

Total RNA from tissues were isolated by the TRIzol RNA isolation protocol. QuantiTect RT kit (Qiagen) was then used to make cDNA from the RNA samples, following manufacturer's instructions.

Relative gene expression was determined by quantitative real-time PCR (qRT-PCR) on a BioRad CFX384 real time system using ABsolute QPCR SYBR Green mix (Thermo Scientific). Gene expression was determined by correcting for reference gene values (36B4), and the calculated values were expressed relative to the control group per experiment. Primer sequences can be found in Table S1.

Western Blotting

Tissues were homogenized in ice-cold RIPA (50 mM Tris pH 8.0, 1% nonidet P40, 0.5% deoxycholate, 0.1% SDS, 150 mM NaCl) containing phosphatase inhibitor cocktail 3 (Sigma-Aldrich), protease inhibitor (Roche Diagnostics), 1 mM phenylmethylsulfonyl fluoride (PMSF; Roche Diagnostics), and 15 mM NaVanadate. Protein concentrations were determined with a DC protein assay kit (Bio-Rad).

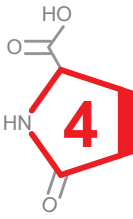

Equal amounts of protein were loaded on 10% polycrylamide gels. After electrophoresis, the gels were blotted onto PVDF membranes. Membranes were then incubated overnight at 4°C with the primary antibody, followed by 1h incubation at room temperature with secondary antibody. Detection was performed by ECL and analyzed with densitometry (ImageQuant LAS4000; GE Healthcare Europe). Antibodies used are described in Table S2.

For the detection of oxidized proteins we utilized the Oxidized Protein Western Blot Kit (Abcam). Tissue samples were homogenized and processed as per manufacturer's instructions. Protein concentrations were measured using the Bradford Protein Assay (Bio-Rad). Briefly, equal amounts of protein were derivatized using 2, 4 dinitrophenyl hydrazine (DNPH) for 15 min at room temperature and then neutralized. The samples were then loaded on a 10% polyacrylamide gels and DNP conjugated proteins were detected by western blotting using primary DNP antibody and HRP conjugated secondary antibody.

Healthy control patient population and study design

As a control group, healthy individuals, included as control population for a previously published study, were used (28). Subjects scheduled for total hip or knee replacement surgery at the University Medical Center Groningen, Groningen, The Netherlands were eligible. Exclusion criteria included the presence of previously diagnosed cardiovascular disease, diabetes mellitus or more than one of the following cardiovascular risk factors: hypertension, smoking, hypercholesterolemia, obesity and physical inactivity. Laboratory measurements were made in venous blood stored at -80°C which was never thawed before assaying. The study protocol was approved by the local ethics committee and the study was conducted in accordance with the Declaration of Helsinki. All subjects gave written informed consent prior to any study-related procedures.

Patient population and study design

The methods and primary results of this study have been reported elsewhere (29–31). Briefly, 52 patients with symptomatic HFpEF and pulmonary hypertension were randomly assigned to either the treatment group (sildenafil 60 mg t.i.d. three times daily) or the placebo group. Eligible patients were male or female, with HFpEF (left ventricular ejection fraction [LVEF] ≥ 45% and New York Heart Association [NYHA] functional class II-IV) and pulmonary hypertension (mean PAP>25mmHg and mean PAWP>15mmHg), which was invasively diagnosed by right-sided cardiac catheterization and two-dimensional echocardiography. The primary objective was to evaluate the effect of 12-week treatment with sildenafil compared to placebo on invasively measure mean pulmonary artery pressure (PAP) in patients with HFpEF and pulmonary hypertension. The secondary objectives were to assess the effects of sildenafil on pulmonary artery wedge pressure (PAWP), cardiac output, and exercise capacity, as measured by cardiopulmonary exercise testing. Overall, results from this study were neutral (29–31).

At baseline patients underwent physical examination, right-sided catheterization, two-dimensional echocardiography, laboratory assessments, and an exercise capacity test, and started with sildenafil or placebo, as previously described (29–31). After 2 weeks patients were titrated to sildenafil or placebo 60 mg t.i.d. The same medical assessment was performed after 12 weeks of treatment, as previously described (29–31). The randomized clinical trial conformed to the Declaration of Helsinki and the Medical Research Involving Human Subjects Act, and was approved by the institutional review board and local Ethics Committee. All patients provided written informed consent. This trial is registered at Clinicaltrails.gov, number NCT01726049.

In this study 51 patient plasma samples at baseline were analyzed, from the 52 previously described, of the remaining patient no plasma was available for 5-oxoproline measurements and was excluded from this analysis. Since sildenafil was found to have no effects on the primary or secondary objectives of the trial, we pooled the patient population to assess the effects of plasma 5-oxoproline levels in the total population on cardiac structure and function.

LC-MS measurements

5-oxoproline internal standard was prepared from ^{13}C-labeled L-glutamic acid as previously described (16). Oxidized glutathione (GSSG) was prepared by a controlled oxidation of ^{13}C, ^{15}N-labeled GSH. Briefly, 10 mg of ^{13}C, ^{15}N-labeled GSH were dissolved in 1 mL water. Half of the solution (0.5 mL) was mixed with of 0.5 mg NaI (final concentration 6.7 mM) and 1 µL 30% H_2O_2. The mixture was heated at 25°C for 60 min to allow oxidation. Excess H_2O_2 was eliminated by increasing the temperature of the mixture to 65°C for 5 min as previously described (32).

For 5-oxoproline measurements were performed on plasma samples from the patients and urine, plasma, and tissue samples from mice,. The sample preparation was performed as previously published (16), with some minor modifications. Briefly, 25 µL sample (urine or plasma) and ±1 mg of powdered tissue was mixed with 200 µL of the extraction solution (0.5 µL IS 5-oxoproline in 75% methanol). Samples were vortex mixed and centrifuged for 10 min at 20,000g. Supernatant was dried under a stream of nitrogen gas at room temperature, followed by resuspension in 100 µL of water. At this stage, samples were stored at -80°C until LC-MS measurements were performed. LC-MS measurements of 5-oxoproline were performed as previously described (16).

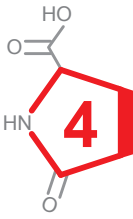

For GSH and GSSG measurements were performed on tissue samples of mice. Murine tissues (cardiac or renal) were prepared by adding 200 µL of cold (-20°C) extraction solution [0.5 µL isotopically-labeled internal standard of GSH and GSSG (ratio of 2:1) and 1.25 mg of N-ethylmaleimide (NEM) in 75% methanol] to ±1 mg of powdered tissue. The mixture was then sonicated for 5 min, followed by incubation for 45 min in a thermomixer at room temperature and 900 rpm to allow derivatization of GSH to GSH-NEM. Samples were centrifuged at 4°C and 20800g for 20 min. The supernatant was collected and dried under a stream of nitrogen at room temperature, followed by resuspension in 100 µL water. At this stage, samples were stored at -80°C until LC-MS measurements were performed. GSH-NEM and GSSG were separated in reverse phase mode on an Acquity HSS T3 column (1.8 µm, 100 × 2.1 mm; Waters) using a 1290 Infinity LC system (Agilent). Formic acid (0.1%) in water was used as eluent A and methanol as eluent B. The following gradient was applied: 0 min – 100%A, 2.5 min – 100%A, 5 min – 95%A, 6 min – 15%A, 8 min – 15%A and 10 min – 100%A. The column temperature was set at 30°C, the flow rate was 0.3 mL/min, and the injection volume was 10 µL.

Mass spectrometry detection was performed using a 6410 Triple Quadrupole MS system (Agilent) by positive electrospray ionization (ESI+) in the Multiple Reaction Monitoring (MRM) mode. The optimized MS source parameters were: ionspray voltage: +1500V, drying gas flow (N2): 6 L/min, drying gas temperature 300°C, nebulizer pressure: 15 psi. The quadrupole mass analyzer was set to unit resolution and the electron multiplier to 2400 V. The run was divided into 2 segments with MS/MS transitions 433/304 for GSH-NEM, 436/307 for ^{13}C, ^{15}N-labeled GSH-NEM (IS), and 613/355 for GSSG, 619/361 for ^{13}C, ^{15}N-labeled GSSG (IS). Fragmentor and collision energies were optimized to 125 V and 9 V for GSH-NEM and 200 V and 21 V for GSSG, respectively. The dwell time for each transition was 100 ms. The LC-MS system was controlled by MassHunter Workstation software (Agilent).

For tissue samples, pellets formed after centrifugation were homogenized in 200 µL ice-cold RIPA buffer (50 mM Tris pH 8.0, 1% Nonidet P40, 0.5% deoxycholate, 0.1% SDS, 150 mM NaCl). Protein concentrations were determined with the Pierce BCA Protein Assay Kit (ThermoFisher Scientific), following the manufacturer's instructions. Tissue concentrations of 5-oxoproline, GSH, and GSSG were normalized to tissue protein concentrations.

Statistical analysis

All animal experimental data is represented as mean values ± standard error of the mean (SEM). To compare the difference between two groups, the Student's t-test was performed. Comparison between more than two groups were done using one-way analysis of variance (ANOVA) with post hoc Bonferroni test. P-values of < 0.05 were considered statistically significant. All analyses were done using GraphPad Prism software V5.04 (GraphPad software, Inc, La Jolla, CA, USA). For the animal experiments, we chose the sample sizes for all the groups based on the feasibility and prior knowledge of statistical power from previously published experiments (16). With small sample sizes we did not apply statistical tests for normality or equality of variances.

Patients from the sildenafil study were divided according to low (below median) and high (above median) levels of 5-oxoproline. To compare clinical characteristics and echocardiographic parameters between patients with low and high levels of 5-oxoproline, the Student's t-test, Mann-Whitney-U test or the chi-2 test was used depending on the nature of the variable. To test for the association between concentric remodeling and 5-oxoprolinase, logistic regression was used with concentric remodeling as the dependent variable. We then subsequently corrected for clinically relevant confounders including age, sex, renal function, BMI, systolic blood pressure and levels of NT-proBNP. All tests were performed 2 sided, and a P value < 0.05 was considered statistically significant. All statistical analyses were performed using STATA version 14.2 (StataCorp LP, College station, Texas, USA).

Results

OPLAH knock-out mice have increased levels of 5-oxoproline

To study the effects of OPLAH depletion *in vivo*, we generated *Oplah* knock-out mice, Oplah$^{tm1a(KOMP)Wtsi}$ (here after referred to as KO) mice (23). Heterozygous (HET) male mice were mated with HET female mice resulting on average in a nest size of 7.8 pups with the mendelian distribution of 32.5% KO, 45.5% HET, and 22.0% wild-type (WT) mice. On mRNA and protein level the expression of OPLAH was ~50% reduced in the HET mice, relative to the expression in the WT littermates

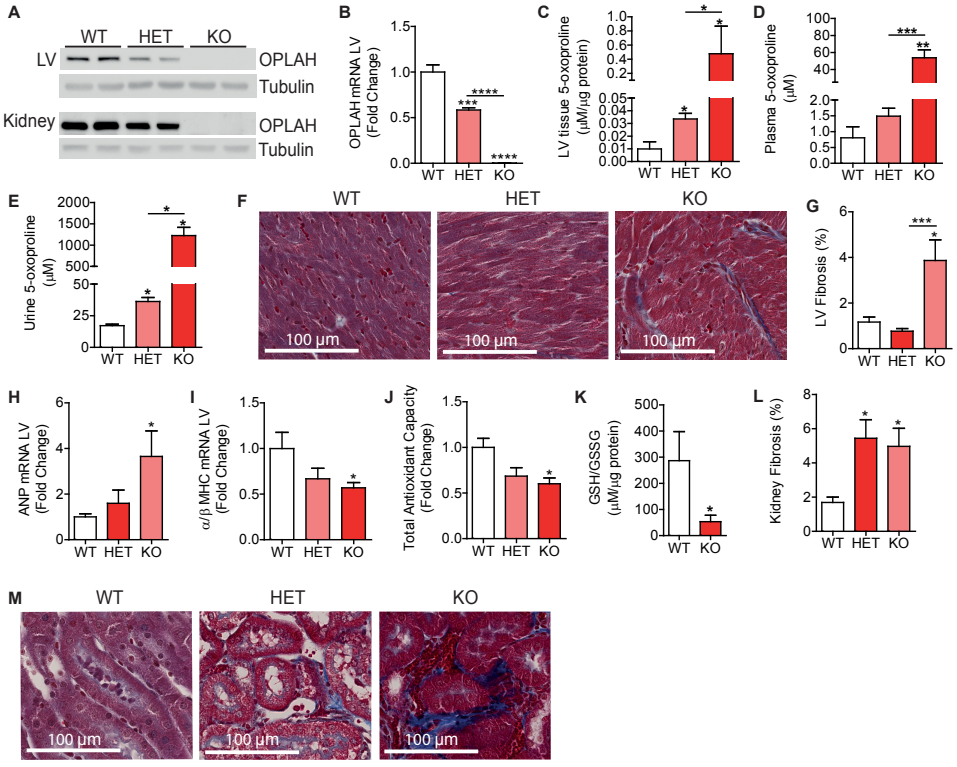

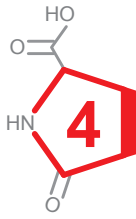

Fig. 1. Baseline characterization of the Oplah knock-out mice.
A. Representative immunoblotting analysis of OPLAH expression in the left ventricle (LV) and kidney of wild-type mice (WT), heterozygous mice (HET), and full body Oplah knock-out mice (KO). **B.** qRT-PCR mRNA expression of OPLAH in the LV of WT (n = 6), HET (n = 7), and KO (n = 5) mice. **C.** LV tissue 5-oxoproline of WT (n = 5), HET (n = 7), and KO (n = 5) mice. **D.** Plasma 5-oxoproline of WT (n = 5), HET (n = 9), and KO (n = 5) mice. **E.** Urine 5-oxoproline of WT, HET, and KO (n = 4) mice. **F.** Representative LV tissue sections with Masson's trichrome of WT, HET and KO mice. **G.** Percent LV fibrosis in WT (n = 6), HET (n = 9) and KO (n = 5) mice. **H.** qRT-PCR mRNA expression of ANP in the LV of WT (n = 5), HET (n = 7) and KO (n = 5) mice. **I.** qRT-PCR mRNA expression of α/β-MHC ratio in the LV of WT (n = 6), HET (n = 7) and KO (n = 5) mice. **J.** LV tissue total antioxidant capacity of WT (n = 4), HET (n = 3) and KO (n = 4) mice. **K.** Ratio of reduced glutathione (GSH) to oxidized glutathione (GSSG) in WT (n = 3) and KO (n = 5) mice. **L.** Percent kidney fibrosis in WT (n = 6), HET (n = 9) and KO (n = 5) mice. **M.** Representative kidney tissue sections with Masson's trichrome staining of WT, HET and KO mice. Data are presented as means ± SEM *, P < 0.05; **, P < 0.01; ***, P < 0.001; ****, P < 0.0001, as calculated by one-way analysis of variance (ANOVA) and Student's T-test.

and absent in the KO mice (Fig. 1A-1B). Since OPLAH is an enzyme involved in converting 5-oxoproline to glutamate, we measured the concentration of left ventricular (LV) tissue, plasma and urine 5-oxoproline in these mice. 5-Oxoproline levels in all samples were significantly elevated in the KO mice, compared to the WT mice (Fig. 1C-1E). HET mice demonstrated a significant increase in LV tissue and urine 5-oxoproline, and a mild non-significant increase in 5-oxoproline levels in the plasma, compared to the WT mice. These findings suggest that a single functional

Table 1. Phenotypic characterization of wild-type (WT), heterozygous (HET), and knock-out (KO) mice.

	WT	HET	KO
Variable	**n = 6**	**n = 9**	**n = 5**
Body weight (tibia corrected), g/cm	17.6 ± 2.5	17.6 ± 2.9	18.5 ± 4.7
Organ weight (tibia corrected), mg/cm			
Atria	3.3 ± 0.4	4.2 ± 0.8*	4.1 ± 0.3*
Right Ventricle	14.6 ± 1.2	14.2 ± 1.9	14.1 ± 1.7
Left Ventricle	61.8 ± 5.5	62.8 ± 9.0	64.9 ± 8.4
Kidney	248.1 ± 29.3	239.8 ± 29.0	267.2 ± 38.6
Liver	822.8 ± 105.1	821.7 ± 119.6	860.1 ± 226.3
Hemodynamic measurements			
Systolic blood pressure (mmHg)	99.6 ± 8.9	99.2 ± 6.9	103.7 ± 8.8
Diastolic blood pressure (mmHg)	67.1 ± 6.8	66.5 ± 6.3	61.1 ± 6.6
LV End systolic pressure (mmHg)	88.9 ± 10.5	88.2 ± 13.8	92.6 ± 12.1
LV End diastolic pressure (mmHg)	5.8 ± 2.9	8.4 ± 4.2	11.3 ± 4.6*
Tau (ms)	6.8 ± 0.8	7.29 ± 1.0	8.5 ± 1.2*
dP/dT max (mmHg/s)	8493.4 ± 1331.1	8023.6 ± 1241.9	7676.5 ± 982.5
dP/dT min (mmHg/s)	-7624.8 ± 1115.7	-7162.5 ± 1397.4	-6624.1 ± 1358.6
Heart rate (BPM)	450.9 ± 23.5	427.0 ± 56.5	455.6 ± 63.5
LV ejection fraction (%)	53.2 ± 2.6	55.3 ± 8.8	54.8 ± 2.9
LV End systolic volume (µL)	24.6 ± 5.5	23.6 ± 8.6	21.3 ± 1.5
LV End diastolic volume (µL)	52.8 ± 11.4	51.6 ± 11.9	50.1 ± 5.9
Stroke volume (µL)	28.2 ± 6.3	27.9 ± 5.6	28.9 ± 4.9

* = P > 0.05 WT VS KO or HET

Oplah gene is sufficient to some extend maintain the homeostasis of 5-oxoproline.

Oplah knock-out mice develop a HFpEF phenotype

Next, we were interested in characterizing if the reduction in OPLAH, and therefore an increase in 5-oxoproline, resulted in a cardiac phenotype. At 20 weeks of age we performed cardiac MRI, hemodynamic measurements and histological analysis on the KO, HET and WT mice. With exception to an increase in atria weight in the KO and HET mice, organ weights were similar to those of the WT littermates (Table 1). Interestingly, in terms of hemodynamic measurements we observed that the KO mice had significantly increased LV end diastolic pressures (LVEDP) [11.3 ± 4.6 mmHg (KO) vs 5.8 ± 2.9 mmHg (WT), P = 0.047] and an increase in the isovolumic relaxation constant (Tau) [8.5 ± 1.2 ms (KO) vs 6.8 ± 0.8 ms (WT), P = 0.037],

with a preserved LV ejection fraction (LVEF) (Table 1). The HET mice demonstrated a similar trend, however these were significantly different from the WT littermates [LVEDP = 8.4 ± 4.2 mmHg (HET) vs 5.8 ± 2.9 mmHg (WT), P = 0.093, Tau = 7.3 ± 1.0 ms (HET) vs 6.8 ± 0.8 ms (WT), P = 0.368]. Histological analysis revealed that the KO mice had increased LV fibrosis, which was coupled to an increase in atrial natriuretic peptide (*Anp*) expression and reduction in α/β myosin heavy chain (MHC) ratio (both of which are markers for increased cardiac injury) (Fig. 1F-1I). The HET mice did not demonstrate an increase in LV fibrosis, nor did they display a significant increase in *Anp* or reduction in α/β MHC ratio. To determine whether the cardiac phenotype was a result of an increase in oxidative stress, we assessed the total antioxidant capacity (TAC) in these mice. The KO mice were found to have a significantly reduced TAC, while the HET demonstrate a non-significant reduction, when compared to the WT littermates (Fig. 1J). It was previously also reported that 5-oxoproline could induce protein oxidation in rat brain tissue (20,21). To test whether this was also the case in these mice, we measured the total protein carbonylation, a well-known marker for oxidative stress and protein oxidation, in the LV of these animals (Fig. S1). The KO mice were found to have a significant increase in total protein carbonyl content, while the HET animals had a mild non-significant increase, when compared to the WT littermates. To further assess the levels of oxidative stress in the KO mice, we measured the reduced to oxidized glutathione (GSH/GSSG) ratio, a well-established indicator for oxidative stress, by means of LC-MS (Fig. 1K). The KO mice were found to have a significant reduction in the GSH/GSSG. These observations are in line with previous reports showing that 5-oxoproline is an oxidative stress inducing agent (16,20,21). Surprisingly, both the KO and HET mice were found to have significantly elevated kidney fibrosis (Fig. 1L-M). Combined these findings demonstrate that the ablation of OPLAH, resulting in increased 5-oxoproline levels, leads to oxidative stress, cardiac fibrosis, atrial enlargement, impaired LV relaxation, increased LV filling pressures, and renal fibrosis with a preserved LVEF. These observations are similar to those observed in patients with HFpEF (33), suggesting a possible link between the OPLAH/5-oxoproline axis and the onset of HFpEF.

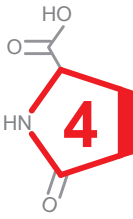

Oplah knock-out mice are more susceptible to cardiac ischemia/reperfusion injury

Following the baseline characterization of the KO mice, we hypothesized that these mice would be more susceptible to cardiac events. Therefore, we performed cardiac ischemia/reperfusion (IR), were the mice underwent 60 min of ischemia followed by 4 weeks of reperfusion. Upon the induction of IR injury there was a dramatic incidence of sudden death in both the KO and HET mice, an effect not observed in the WT littermates [survival rate 47.6%, 68.8% and 84.6%, respectively (Fig. 2A)]. To assess why this significant incidence of sudden death occurred in the KO mice, when compared to the WT mice (P = 0.03), we performed ECG measurement during

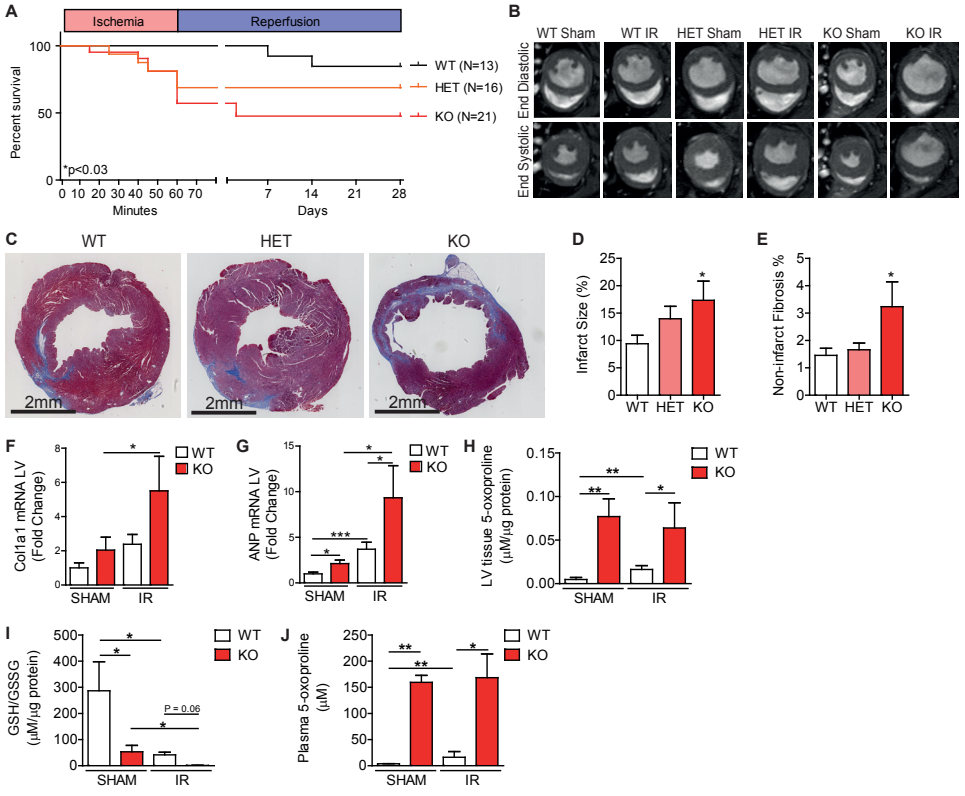

Fig. 2. Oplah knock-out mice are more susceptible to cardiac ischemia/reperfusion (IR) injury. **A.** Survival data of wild-type (WT, n = 13), heterozygous (HET, n = 16) and Oplah knock-out (KO, n = 21) mice following the implementation of IR injury. **B.** Representative cardiac MRI images of WT, HET and KO mice hearts. **C.** Representative LV tissue sections with Masson's trichrome staining of WT, HET and KO mice with cardiac IR injury. **D-E.** Quantified LV infarct size (**D**) and non-infarct fibrosis (**E**) of WT (n = 11), HET (n = 8) and KO (n = 8) post-IR injury. **F.** qRT-PCR analysis of LV mRNA for Collagen type 1, alpha 1 (*Col1a1*) (WT SHAM n = 15, WT IR n = 11, KO SHAM n = 14, KO IR n = 10). **G.** qRT-PCR analysis of LV mRNA for Atrial natriuretic peptide (*Anp*) (WT SHAM n = 15, WT IR n = 11, KO SHAM n = 14, KO IR n = 10). **H.** LV tissue 5-oxoproline levels (WT SHAM n = 11, WT IR n = 11, KO SHAM n = 6, KO IR n = 4). **I.** Ratio of reduced glutathione (GSH) to oxidized glutathione (GSSG) in LV tissue (WT SHAM n = 3, WT IR n = 4, KO SHAM n = 5, KO IR n = 3). **J.** Plasma 5-oxoproline levels (WT SHAM n = 11, WT IR n = 11, KO SHAM n = 6, KO IR n = 3). Data are presented as means ± SEM *, P < 0.05; **, P < 0.01; ***, P < 0.001, as calculated by one-way analysis of variance (ANOVA) and Student's T-test. In (A) as calculated by Log-rank (Mantel-Cox) Test.

the ischemic phase. We found no incidence of ventricular tachycardia or ventricular fibrillation (Figure S2A). Furthermore, we also did not observe cardiac tamponade (also known as cardiac rupture or free wall rupture) in the KO mice that perished during the procedure. (Figure S2B-S2D). The KO animals that did die had an ECG with a dying heart pattern, characterized by an extreme bradycardia, widening of the QRS complexes and a decrease in R amplitude, leading to asystole. The KO mice that survived the procedure, seemed to have similar cardiac electrical activity as the

WT littermates. The incidence of sudden death in the KO mice is not a result from tachyarrhythmias, but rather of a dying heart

Oplah knock-out mice have more cardiac and renal damage following cardiac ischemia/reperfusion injury

To assess what the effect of IR injury were on the surviving KO mice, cardiac MRI and PV-loop analysis were performed 4 weeks after the induction of IR. The surviving KO mice had a substantially worsened cardiac function post-IR, compared to the HET and WT mice, as measured by LVEF and stroke volume (Fig. 2B and Table 2). Furthermore, we observed a significant enlargement of the atria, LV, kidney, and liver of the KO mice exposed to IR-injury (Table 2). Histological analysis of the LV demonstrated that the KO mice had significantly larger infarct sizes compared to WT [17.3 ± 9.9% vs 10.4 ± 5.2%, respectively, p=0.043 (Fig. 2C-2D)], coupled to an increase in non-infarcted fibrosis [3.2 ± 2.6% vs 1.2 ± 0.9%, respectively, P = 0.045 (Fig. 2E)]. Following IR injury, the KO mice were also found to have a significant increase in cell size, as measured by means of FITC-labeled WGA staining, an effect not observed in the WT or HET mice (Fig. S3). The effects of IR injury on the HET mice were comparable to those observed in the WT mice, with no significant differences in terms of cardiac function, infarct size and organ weights (Fig. 2C-2E and Table 2).

To further characterize the increase in cardiac fibrosis observed in the KO mice, we measured the expression of several fibrosis markers; collagen type 1 (*Col1a1*), collagen type 3 (*Col1a3*), TIMP metallopeptidase inhibitor 1 (*Timp-1*), matrix metalloproteinase 2 (*Mmp-2*), matrix metalloproteinase 9 (*Mmp-9*), Galectin-3 (*Gal-3*), Procollagen C-endopeptidase enhancer 1 (*Pcolce*), and interleukin 1 receptor-like 1 (*Il1rl1*, also known as *St2*) in cardiac tissue. The KO mice were found to have a significant increase in *Col1a1*, *Col1a3*, *Gal-3*, *Pcolce*, and *Il1rl1*, when compared to the WT mice post-IR injury (Fig. 2F and Fig. S4A-D). Interestingly, the KO mice also had an increase in *Timp-1*/*Mmp-2* and *Timp-1*/*Mmp-9* ratios (Fig. S4E-S4I). These findings suggest that within the KO mice there is a shift from fibrosis breakdown to production. Furthermore, the KO mice also demonstrated an increased Anp expression levels when compared to the WT littermates (Fig. 2G). Besides the evident increase in cardiac fibrosis, we also observed that the KO mice had a substantial increase in LV tissue 5-oxoproline levels, coupled to an increase in oxidative stress as measured by means of the GSH/GSSG ratio (Fig. 2H-2I). Furthermore, the plasma 5-oxoproline levels were also elevated in the KO mice (Fig. 2J). Interestingly, in both the cardiac tissue and plasma we observed an increase in 5-oxoproline levels in the WT mice following IR injury, which coincides with an increase in cardiac tissue oxidative stress (Fig. 2H-2J).

Table 2. Characteristics of wild-type (WT), heterozygous (HET) and knock-out (KO) mice at baseline (Sham) and post-ischemia/reperfusion (IR) injury.

	WT		HET		KO	
Variable	**Sham (n = 15)**	**IR (n = 11)**	**Sham (n = 22)**	**IR (n = 11)**	**SHAM (n = 16)**	**IR (n = 10)**
Body weight (tibia corrected), g/cm	17.7 ± 2.2	17.6 ± 1.1	18.4 ± 2.7	19.2 ± 1.5	18.1 ± 2.9	18.6 ± 1.3
Organ weight (tibia corrected), mg/cm						
Atria	3.5 ± 0.6	4.4 ± 0.6*	4.1 ± 0.8#	3.6 ± 0.7	4.2 ± 0.9#	5.5 ± 0.9**,#
Right Ventricle	13.8 ± 1.5	15.4 ± 1.2*	14.2 ± 1.9	15.5 ± 3.3	14.4 ± 1.9	16.4 ± 2.3*
Left Ventricle	61.3 ± 5.4	72.0 ± 3.9****	64.9 ± 3.9	68.4 ± 5.8	64.6 ± 6.2	83.0 ± 11.0****,#
Kidney	239.5 ± 30.4	241.8 ± 16.7	247.0 ± 34.3	266.6 ± 24.8*	244.8 ± 29.3	284.7 ± 29.3*,#
Liver	850.2 ± 105.3	857.2 ± 32.5	873.4 ± 137.0	922.5 ± 89.9	868.0 ± 134.3	1059.8 ± 137.9**,##
Hemodynamic measurements						
Systolic blood pressure (mmHg)	99.0 ± 9.6	97.1 ± 10.3	100.7 ± 6.3	103.9 ± 9.0	99.7 ± 12.6	98.2 ± 5.2
Diastolic blood pressure (mmHg)	65.8 ± 5.9	66.1 ± 9.4	65.9 ± 5.3	67.5 ± 8.4	60.8 ± 13.9	65.8 ± 5.3
LV End systolic pressure (mmHg)	94.4 ± 10.2	97.9 ± 9.5	93.7 ± 11.5	91.9 ± 13.9	92.4 ± 15.2	94.8 ± 6.3
LV End diastolic pressure (mmHg)	5.5 ± 3.8	15.9 ± 4.3****	9.6 ± 5.1#	14.8 ± 5.9*	9.3 ± 3.4#	16.2 ± 2.3****
Tau (ms)	7.1 ± 1.4	10.4 ± 2.8***	7.6 ± 1.6	9.1 ± 2.0*	8.5 ± 1.2#	9.3 ± 2.2
dP/dT max (mmHg/s)	8210.4 ± 1297.0	7046.5 ± 1418.5	7837.8 ± 1140.8	7494.9 ± 1247.9	7287.4 ± 967.9	6983.8 ± 956.7
dP/dT min (mmHg/s)	-7543.6 ± 1520.1	-5473.3 ± 1172.2 **	-7097.9 ± 1343.9	-6018.7 ± 1427.4	-6419.3 ± 1071.6	-5811.1 ± 978.7
Heart rate (BPM)	454.3 ± 27.5	477.2 ± 41.7	433.6 ± 53.0	462.9 ± 44.5	463.3 ± 54.0	488.2 ± 47.0
LV ejection fraction (%)	49.2 ± 5.6	42.0 ± 7.4*	54.7 ± 7.9	42.7 ± 11.7**	51.7 ± 8.9	33.9 ± 8.4**,#
LV End systolic volume (µL)	27.6 ± 6.9	38.8 ± 12.9*	24.4 ± 7.4	39.6 ± 18.9*	26.4 ± 10.2	44.1 ± 19.3*
LV End diastolic volume (µL)	54.0 ± 9.9	66.1 ± 16.4*	53.0 ± 9.8	66.8 ± 18.3*	53.3 ± 12.2	66.1 ± 20.4
Stroke volume (µL)	26.4 ± 4.8	27.3 ± 5.7	28.6 ± 4.7	27.2 ± 4.2	27.0 ± 4.9	21.9 ± 1.9*,#

* = p>0.05 Sham VS IR

** = p>0.01 Sham VS IR

*** = p>0.001 Sham VS IR

**** = p>0.0001 Sham VS IR

= p>0.05 WT VS KO or HET

= p>0.01 WT VS KO or HET

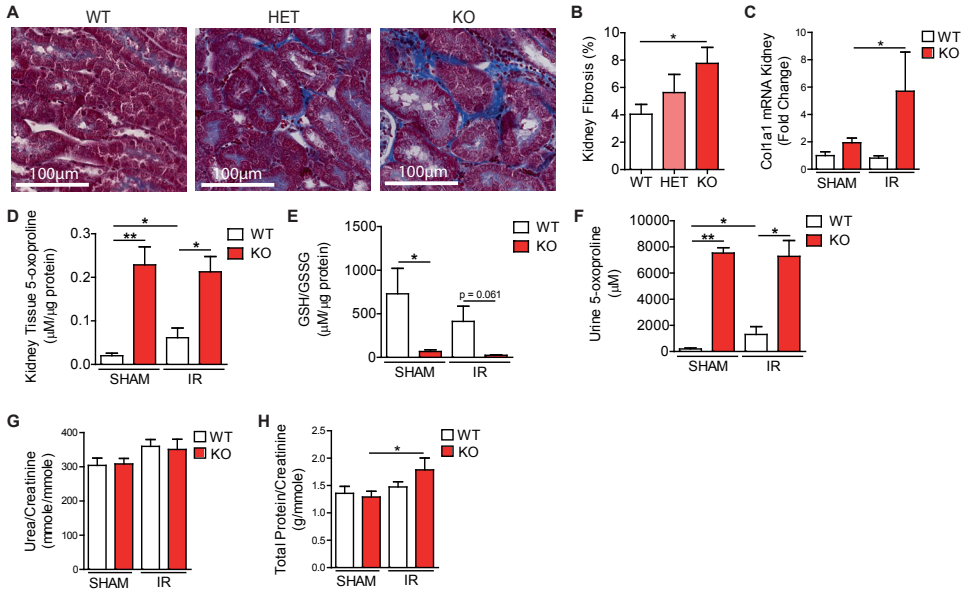

Fig. 3. Oplah knock-out mice develop increased renal damage following cardiac ischemia/reperfusion (IR) injury.
A. Representative kidney tissue sections with Masson's trichrome staining of WT, HET and KO mice with cardiac IR injury. **B.** Quantification of percent kidney fibrosis (WT n = 11, HET n = 11, KO n = 8). **C.** qRT-PCR analysis of kidney mRNA for Collagen type 3, alpha 1 (*Col3a1*) (WT SHAM n = 10, WT IR n = 9, KO SHAM n = 15, KO IR n = 10). **D.** Kidney tissue 5-oxoproline (WT SHAM n = 11, WT IR n = 11, KO SHAM n = 6, KO IR n = 3). **E.** Ratio of reduced glutathione (GSH) to oxidized glutathione (GSSG) in kidney tissue (WT SHAM n = 3, WT IR n = 11, KO SHAM n = 4, KO IR n = 3). **F.** Urine 5-oxoproline (WT SHAM n = 11, WT IR n = 11, KO SHAM n = 6, KO IR n = 3). **G.** Urinary urea to creatinine ratio (WT SHAM n = 11, WT IR n = 10, KO SHAM n = 9, KO IR n = 7). **H.** Urinary total protein to creatinine ratio (WT SHAM n = 11, WT IR n = 10, KO SHAM n = 9, KO IR n = 7). Data are presented as means ± SEM *, P < 0.05; **, P < 0.01, as calculated by one-way analysis of variance (ANOVA) and Student's T-test.

Since at baseline we observed that the KO and HET mice had an increase in renal fibrosis, we also assessed renal fibrosis following IR injury in these mice. We observed that the KO mice had a significant increase in renal fibrosis compared to the WT littermates, while the HET only demonstrate a mild non-significant increase (Fig. 3A-3B).The kidneys of the KO mice were also found to have increased expression of fibrotic markers *Col1a1* and an increase in the *Timp-1*/*Mmp-2* and *Timp-1*/*Mmp-9* (Fig. 3C and Fig. S5A-S5E). Furthermore, we also found the kidneys of the KO mice to have increased expression of *Il1rl1*, when compared to the WT mice (Fig. S4F). These findings suggest that similar to the heart, in the kidneys there also seems to be a switch towards increased fibrosis deposition. Interestingly, we also observed an increase in renal 5-oxoproline levels and oxidative stress (Fig. 3D-3E). To further characterize the effect OPLAH depletion has on kidney function, we measured the 5-oxoproline levels, urea/creatinine and total protein/creatinine ratios in the urine of

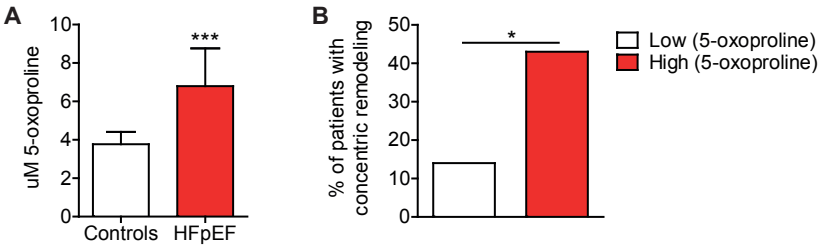

Fig. 4. 5-oxoproline in patients with HFpEF.
A. 5-oxoproline concentrations in healthy controls (controls, n = 6) compared to patients with HFpEF (n = 51). **B.** Percentage of HFpEF patients with left ventricular concentric remodeling according to levels of 5-oxoproline above (High, 6.7 – 12.8 μM, n = 25) and below (Low, 3.7 – 6.7 μM, n = 26) the median. In (**A**) data are presented as means ± SEM ***, P < 0.001, as calculated by Student's t test. In (**B**) data are presented as percentages *, P < 0.05, as calculated by Student's t test.

our mice (Fig. 3F-3H). 5-Oxoproline levels were found to be significantly elevated in the urine of the KO mice, and the WT mice demonstrated an increase in urine 5-oxoproline following IR injury. No significant differences were observed in the urea/creatinine ratio between the KO and WT mice . However, the KO mice were found to have an increase in total protein/creatinine ratio following cardiac IR injury compared to WT. Combined these findings suggest that mice lacking OPLAH, are not only more susceptible to cardiac injury when challenged with IR, but also to renal injury.

5-oxoproline in plasma of HFpEF patients

Plasma 5-oxoproline was measured in 6 healthy controls (Table S3) and in a cohort of 51 HFpEF patients (Table S4). We found plasma 5-oxoproline levels to be ±2-fold higher in the HFpEF patients compared to healthy controls (6.8 ± 1.9 μM vs 3.8 ± 0.6 μM, respectively, P = 0.0001) (Fig. 4A). To further address the involvement of 5-oxoproline within the patient HFpEF patient cohort, we compared clinical charateristics and echocardiographic parameters between patients with high (above the median) and low (below the median) levels of 5-oxoproline. The data on echocardiography measurements of the HFpEF patient cohort are presented in Table 3. Within this cohort of HFpEF patients we observed equal levels of plasma 5-oxoproline in men and women (p = 0.273). Overall, patients with high 5-oxoproline levels had almost double the prevalence of concentric remodeling (14% vs. 43%, p= 0.040, Fig. 3B). When additionally correcting for age, sex, BMI and levels of NT-proBNP, levels of 5-oxoprolinase remained independently associated with more concentric remodeling (Odds ratio:1.55; 95%CI 1.03-2.33; p=0.038). This observations suggests that OPLAH and 5-oxoproline are not only involved in HFpEF in the murine setting, but also in the clinical manifestation of the disease.

Table 3. Echocardiographic characteristics by 5-oxoproline concentration

	5-oxoproline (3.7 - 6.7 µM)	5-oxoproline (6.7 - 12.8 µM)	
Factor	**n = 26**	**n = 25**	**P value**
Left ventricular ejection fraction, %	60.0 (55.0, 60.0)	60.0 (60.0, 60.0)	0.47
Left ventricular end diastolic diameter, mm	48.0 (44.0, 52.0)	46.0 (43.0, 51.0)	0.69
Left ventricular posterior wall thickness, mm	9.0 (8.0, 9.0)	10.0 (9.0, 11.0)	0.020
Intraventricular septum thickness, mm	11.0 (9.0, 12.0)	11.0 (9.5, 12.0)	0.39
e' lateral, cm/s	8.3 (5.9, 9.7)	8.5 (7.2, 13.7)	0.20
E/e' ratio	13.4 (11.1, 20.3)	11.8 (10.0, 16.6)	0.24
Isovolumetric relaxation time, ms	89.0 (74.0, 94.0)	77.0 (69.0, 89.0)	0.26
TAPSE, mm	19.0 (17.0, 22.0)	18.0 (16.0, 21.0)	0.39
Concentric remodeling, %	14	43	0.04

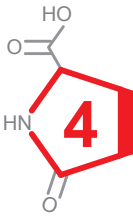

Discussion

HF is one the most challenging health problems of the developed world, with a five year survival rate of less than 50% (2). Nearly half of all patients with HF symptoms, have a preserved ejection fraction which is characterized by renal damage, cardiac stiffening, increased oxidative stress, and atrial enlargement (2,33). Due to the fact that HFpEF patients generally are afflicted with multiple comorbidities [including obesity, hypertension, renal disease, atrial fibrillation, metabolic syndrome, and diabetes mellitus (33)], it is difficult to discern the underlying cardiac pathophysiology leading to the disease. Therefore it is essential to develop novel animal models to help uncover the pathophysiological pathways implicated in this disease (4).

In the field of cardiovascular research most of the HF animal models currently employed are representative of HFrEF, although several models have been proposed that mimic HFpEF. Most of these animal models currently available attempt to reproduce the typical causes of diastolic dysfunction in HFpEF, namely ageing [i.e. FVB/N mice (34)], diabetes mellitus [i.e. db/db mice (35) and ob/ob mice (36)] and hypertension [i.e. aortic constriction (37) and DOCA-Salt mice (38)]. However, these animal models are unable to recapitulate all the features present in the human disease. Furthermore, in most cases these animal models eventually lead to the development of HFrEF (3), whereas in the clinical setting patients diagnosed with HFpEF only transitions into HFrEF with an additional cardiac event (i.e. myocardial infarction, coronary artery disease) (39–41). As such these animal models have limitations for preclinical evaluation of potentially novel therapeutic strategies.

One of the proposed pathophysiological pathways implicated in HFpEF is an increase in oxidative stress (33,42,43). The increase in ROS production has been shown to induce a hypophosphorylation of titin, leading to increased resting tension of cardiomyocytes (a characteristic of increased myocardial passive stiffness) (44-46). Excess ROS production also results in inflammation and cardiomyocyte stress (44,45). Furthermore, ROS has been shown to increase collagen deposition leading to fibrosis (5). These observations suggest that oxidative stress may play an important role in the onset of HFpEF.

The involvement of OPLAH in the heart, and in particular in HF, has only recently been described (16). OPLAH is an enzyme involved in the γ-Glutamyl cycle, where it is responsible for the conversion of 5-oxoproline, a degradation product of Glutathione, back into glutamate (6,19). Previous studies have demonstrated that 5-oxoproline is an oxidative stress inducing agent, thus OPLAH has an antioxidant function by removing this metabolite (16,20,21). In this study we further characterized the role of OPLAH and its substrate 5-oxoproline in HF, with a specific focus on HFpEF. At baseline OPLAH ablation in mice resulted in increased 5-oxoproline, oxidative stress, atrial enlargement, fibrosis, ventricular filling pressures, and impaired LV relaxation coupled to a preserved LV ejection fraction. Interestingly, at baseline the *Oplah* KO mice did not only develop a cardiac phenotype, but we also observed an increase in renal fibrosis, suggesting the increase in 5-oxorpoline was resulting in renal damage. This is of particular interest, since one of the well characterized non-cardiac comorbidities of patients with HFpEF is renal failure (2). Furthermore, we also found that both the heart and the kidneys of the KO mice had higher expression of *St2*, a known marker for inflammation and fibrosis, with a strong link to clinical HFpEF (47–49). Interestingly, when challenged, these mice were found to be more susceptible to cardiac damage and sudden death, following cardiac IR injury. This observation is in line with the observations that HFpEF patients exposed to a cardiac event have an increase incidence of sudden death (39–41). Furthermore, genetic disruption of *Oplah* not only lead to an increase in cardiac damage, but we also observed that the *Oplah* KO mice developed proteinuria following IR injury. Taken together the observed cardiac and renal phenotype in the *Oplah* KO mice, suggests that complete disruption of *Oplah* leads to changes resembling clinical HFpEF (Table S5). Combined with previous findings, that OPLAH overexpression has a cardio protective effect (16), suggest future efforts should be made in identifying compounds with the capacity to indue OPLAH expression or activity. This could lead to novel therapeutic strategies for HF patients, and more interestingly for HFpEF patients.

To further establish the link between our *Oplah* KO mice and HFpEF, we measured

the levels of circulating 5-oxoproline in a cohort of HFpEF patients. We found 5-oxoproline to be significantly elevated in HFpEF patients, when compared to healthy controls. Furthermore, higher levels of circulating 5-oxoproline were found to independently associate with more concentric remodeling, a hallmark of HFpEF.

Although our proposed murine model for HFpEF strongly mimics the development of this disease in the human setting, there remain several limitations to this model. The main limitation is that in this model HFpEF is developed as a result of direct genetic manipulation. Thus, it is uncertain whether the pathophysiological pathway, implicating OPLAH and 5-oxoproline, is also involved in the onset of HFpEF in humans. Rather one could also speculate that the effects we observe in the *Oplah* KO mice are a result of the severe oxidative stress, due to accumulation of the oxidative stress inducing agent 5-oxoproline. Another limitation is that following the induction of IR injury, there was a drastic incidence of sudden death in the *Oplah* KO mice, therefore any analysis performed on the surviving KO mice is an underestimation of severity of cardiac injury on these mice. Furthermore, the surviving mice transitioned into a HFrEF phenotype, with reduce LV ejection fraction. These observation are in line with previous clinical studies which found that following a cardiac event, HFpEF patients would transition into HFrEF and had an increased incidence of sudden death (39–41). Therefore, it would be of interest to perform an RNA sequencing analysis on these animals to maybe shed some new light on possible pathophysiological pathways involved in the onset of HFpEF in these animals at baseline and how this shifts to a HFrEF phenotype following IR injury. Additionally, circulating 5-oxoproline was measured in a very specific cohort of HFpEF patients with pulmonary hypertension, and therefore it is uncertain to which extent findings of this patient cohort can be extrapolated to other patients with HFpEF. Furthermore, the sample size was rather small, inhibiting us from performing more extensive analyses.

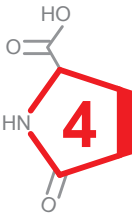

Acknowledgments

We thank Martin Dokter and Kees van de Kolk for their excellent technical assistance.

References

1. Owens AT, Brozena SC, Jessup M. New Management Strategies in Heart Failure. Circ Res American Heart Association, Inc.; 2016;118:480–495.
2. Ponikowski P, Voors AA, Anker SD, Bueno H, Cleland JGF, Coats AJS, Falk V, González-Juanatey JR, Harjola V-P, Jankowska EA, Jessup M, Linde C, Nihoyannopoulos P, Parissis JT, Pieske B, Riley JP, Rosano GMC, Ruilope LM, Ruschitzka F, Rutten FH, Meer P van der, Authors/Task Force Members, Document Reviewers. 2016 ESC Guidelines for the diagnosis and treatment of acute and chronic heart failure. Eur J Heart Fail 2016;18:891–975.
3. Conceição G, Heinonen I, Lourenço AP, Duncker DJ, Falcão-Pires I. Animal models of heart failure with preserved ejection fraction. Netherlands Hear J Bohn Stafleu van Loghum; 2016;24:275–286.
4. Roh J, Houstis N, Rosenzweig A. Why Don't We Have Proven Treatments for HFpEF? Circ Res American Heart Association, Inc.; 2017;120:1243–1245.
5. Paulus WJ, Tschöpe C. A Novel Paradigm for Heart Failure With Preserved Ejection Fraction. J Am Coll Cardiol 2013;62:263–271.
6. Liu Y, Hyde AS, Simpson MA, Barycki JJ. Emerging regulatory paradigms in glutathione metabolism. Adv Cancer Res 2014;122:69–101.
7. Stanley BA, Sivakumaran V, Shi S, McDonald I, Lloyd D, Watson WH, Aon MA, Paolocci N. Thioredoxin reductase-2 is essential for keeping low levels of H(2)O(2) emission from isolated heart mitochondria. J Biol Chem American Society for Biochemistry and Molecular Biology; 2011;286:33669–33677.
8. Aon MA, Stanley BA, Sivakumaran V, Kembro JM, O'Rourke B, Paolocci N, Cortassa S. Glutathione/thioredoxin systems modulate mitochondrial H2O2 emission: an experimental-computational study. J Gen Physiol The Rockefeller University Press; 2012;139:479–491.
9. Hoshino Y, Shioji K, Nakamura H, Masutani H, Yodoi J. From Oxygen Sensing to Heart Failure: Role of Thioredoxin. Antioxid Redox Signal Mary Ann Liebert, Inc. 2 Madison Avenue Larchmont, NY 10538 USA ; 2007;9:689–699.
10. Chen C, Chen H, Zhou HJ, Ji W, Min W. Mechanistic Role of Thioredoxin 2 in Heart Failure. Advances in experimental medicine and biology 2017. p. 265–276.
11. Whayne TF, Parinandi N, Maulik N. Thioredoxins in cardiovascular disease. Can J Physiol Pharmacol 2015;93:903–911.
12. Kobayashi T, Watanabe Y, Saito Y, Fujioka D, Nakamura T, Obata J, Kitta Y, Yano T, Kawabata K, Watanabe K, Mishina H, Ito S, Kugiyama K. Mice lacking the glutamate-cysteine ligase modifier subunit are susceptible to myocardial ischaemia-reperfusion injury. Cardiovasc Res 2010;85:785–795.
13. Nakamura S, Kugiyama K, Sugiyama S, Miyamoto S, Koide S, Fukushima H, Honda O, Yoshimura M, Ogawa H. Polymorphism in the 5'-flanking region of human glutamate-cysteine ligase modifier subunit gene is associated with myocardial infarction. Circulation 2002;105:2968–2973.
14. Shiomi T, Tsutsui H, Matsusaka H, Murakami K, Hayashidani S, Ikeuchi M, Wen J, Kubota T, Utsumi H, Takeshita A. Overexpression of glutathione peroxidase prevents left ventricular remodeling and failure after myocardial infarction in mice. Circulation 2004;109:544–549.
15. Zhang Y, Handy DE, Loscalzo J. Adenosine-dependent induction of glutathione peroxidase 1 in human primary endothelial cells and protection against oxidative stress. Circ Res American Heart Association, Inc.; 2005;96:831–837.
16. Pol A van der, Gil A, Silljé HHW, Tromp J, Ovchinnikova ES, Vreeswijk-Baudoin I, Hoes M, Domian IJ, Sluis B van de, Deursen JM van, Voors AA, Veldhuisen DJ van, Gilst WH van, Berezikov E, Harst P van der, Boer RA de, Bischoff R, Meer P van der. Accumulation of 5-oxoproline in myocardial dysfunction and the protective effects of OPLAH. Sci Transl Med 2017;9:eaam8574.
17. Galasso G, Schiekofer S, Sato K, Shibata R, Handy DE, Ouchi N, Leopold JA, Loscalzo J, Walsh K. Impaired angiogenesis in glutathione peroxidase-1-deficient mice is associated with endothelial progenitor cell dysfunction. Circ Res American Heart Association, Inc.; 2006;98:254–261.
18. Damy T, Kirsch M, Khouzami L, Caramelle P, Corvoisier P Le, Roudot-Thoraval F, Dubois-Randé J-L, Hittinger L, Pavoine C, Pecker F. Glutathione deficiency in cardiac patients is related to the functional status and structural cardiac abnormalities. PLoS One 2009;4:e4871.
19. Meister A, Anderson ME. Glutathione. Annu Rev Biochem Annual Reviews 4139 El Camino Way, P.O. Box 10139, Palo Alto, CA 94303-0139, USA ; 1983;52:711–760.
20. Pederzolli CD, Sgaravatti AM, Braum CA, Prestes CC, Zorzi GK, Sgarbi MB, Wyse ATS, Wannmacher

CMD, Wajner M, Dutra-Filho CS. 5-Oxoproline reduces non-enzymatic antioxidant defenses in vitro in rat brain. Metab Brain Dis 2007;22:51–65.
21. Pederzolli CD, Mescka CP, Zandoná BR, Moura Coelho D de, Sgaravatti AM, Sgarbi MB, Souza Wyse AT de, Duval Wannmacher CM, Wajner M, Vargas CR, Dutra-Filho CS. Acute administration of 5-oxoproline induces oxidative damage to lipids and proteins and impairs antioxidant defenses in cerebral cortex and cerebellum of young rats. Metab Brain Dis 2010;25:145–154.
22. Yang K-C, Yamada KA, Patel AY, Topkara VK, George I, Cheema FH, Ewald GA, Mann DL, Nerbonne JM. Deep RNA sequencing reveals dynamic regulation of myocardial noncoding RNAs in failing human heart and remodeling with mechanical circulatory support. Circulation 2014;129:1009–1021.
23. Skarnes WC, Rosen B, West AP, Koutsourakis M, Bushell W, Iyer V, Mujica AO, Thomas M, Harrow J, Cox T, Jackson D, Severin J, Biggs P, Fu J, Nefedov M, Jong PJ de, Stewart AF, Bradley A. A conditional knockout resource for the genome-wide study of mouse gene function. Nature Nature Research; 2011;474:337–342.
24. Ryder E, Gleeson D, Sethi D, Vyas S, Miklejewska E, Dalvi P, Habib B, Cook R, Hardy M, Jhaveri K, Bottomley J, Wardle-Jones H, Bussell JN, Houghton R, Salisbury J, Skarnes WC, Ramirez-Solis R, Ramirez-Solis R. Molecular Characterization of Mutant Mouse Strains Generated from the EUCOMM/KOMP-CSD ES Cell Resource. Mamm Genome Springer US; 2013;24:286–294.
25. Karp NA, Meehan TF, Morgan H, Mason JC, Blake A, Kurbatova N, Smedley D, Jacobsen J, Mott RF, Iyer V, Matthews P, Melvin DG, Wells S, Flenniken AM, Masuya H, Wakana S, White JK, Lloyd KCK, Reynolds CL, Paylor R, West DB, Svenson KL, Chesler EJ, Angelis MH de, Tocchini-Valentini GP, Sorg T, Herault Y, Parkinson H, Mallon A-M, Brown SDM. Applying the ARRIVE Guidelines to an In Vivo Database. PLOS Biol 2015;13:e1002151.
26. Booij HG, Yu H, Boer RA De, Kolk CWA van de, Sluis B van de, Deursen JM Van, Gilst WH Van, Silljé HHW, Westenbrink BD. Overexpression of A kinase interacting protein 1 attenuates myocardial ischaemia/reperfusion injury but does not influence heart failure development. Cardiovasc Res 2016;111.
27. Schindelin J, Arganda-Carreras I, Frise E, Kaynig V, Longair M, Pietzsch T, Preibisch S, Rueden C, Saalfeld S, Schmid B, Tinevez J-Y, White DJ, Hartenstein V, Eliceiri K, Tomancak P, Cardona A. Fiji: an open-source platform for biological-image analysis. Nat Methods 2012;9:676–682.
28. Grote Beverborg N, Klip IjT, Meijers WC, Voors AA, Vegter EL, Wal HH van der, Swinkels DW, Pelt J van, Mulder AB, Bulstra SK, Vellenga E, Mariani MA, Boer RA de, Veldhuisen DJ van, Meer P van der. Definition of Iron Deficiency Based on the Gold Standard of Bone Marrow Iron Staining in Heart Failure Patients. Circ Heart Fail 2018;11:e004519.
29. Hoendermis ES, Liu LCY, Hummel YM, Meer P van der, Boer RA de, Berger RMF, Veldhuisen DJ van, Voors AA. Effects of sildenafil on invasive haemodynamics and exercise capacity in heart failure patients with preserved ejection fraction and pulmonary hypertension: a randomized controlled trial. Eur Heart J 2015;36:2565–2573.
30. Liu LCY, Hummel YM, Meer P van der, Berger RMF, Damman K, Veldhuisen DJ van, Voors AA, Hoendermis ES. Effects of sildenafil on cardiac structure and function, cardiopulmonary exercise testing and health-related quality of life measures in heart failure patients with preserved ejection fraction and pulmonary hypertension. Eur J Heart Fail 2017;19:116–125.
31. Lam CSP, Rienstra M, Tay WT, Liu LCY, Hummel YM, Meer P van der, Boer RA de, Gelder IC Van, Veldhuisen DJ van, Voors AA, Hoendermis ES. Atrial Fibrillation in Heart Failure With Preserved Ejection Fraction: Association With Exercise Capacity, Left Ventricular Filling Pressures, Natriuretic Peptides, and Left Atrial Volume. JACC Heart Fail 2017;5:92–98.
32. Haberhauer-Troyer C, Delic M, Gasser B, Mattanovich D, Hann S, Koellensperger G. Accurate quantification of the redox-sensitive GSH/GSSG ratios in the yeast Pichia pastoris by HILIC-MS/MS. Anal Bioanal Chem 2013;405:2031–2039.
33. Sharma K, Kass DA. Heart Failure With Preserved Ejection Fraction: Mechanisms, Clinical Features, and Therapies. Circ Res 2014;115:79–96.
34. Koch SE, Haworth KJ, Robbins N, Smith MA, Lather N, Anjak A, Jiang M, Varma P, Jones WK, Rubinstein J. Age- and gender-related changes in ventricular performance in wild-type FVB/N mice as evaluated by conventional and vector velocity echocardiography imaging: a retrospective study. Ultrasound Med Biol 2013;39:2034–2043.
35. Mori J, Patel VB, Abo Alrob O, Basu R, Altamimi T, Desaulniers J, Wagg CS, Kassiri Z, Lopaschuk GD, Oudit GY. Angiotensin 1-7 ameliorates diabetic cardiomyopathy and diastolic dysfunction in db/db mice by reducing lipotoxicity and inflammation. Circ Heart Fail 2014;7:327–339.

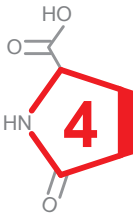

36. Bergh A Van den, Vanderper A, Vangheluwe P, Desjardins F, Nevelsteen I, Verreth W, Wuytack F, Holvoet P, Flameng W, Balligand J-L, Herijgers P. Dyslipidaemia in type II diabetic mice does not aggravate contractile impairment but increases ventricular stiffness. Cardiovasc Res Oxford University Press; 2008;77:371–379.
37. Litwin SE, Katz SE, Weinberg EO, Lorell BH, Aurigemma GP, Douglas PS. Serial echocardiographic-Doppler assessment of left ventricular geometry and function in rats with pressure-overload hypertrophy. Chronic angiotensin-converting enzyme inhibition attenuates the transition to heart failure. Circulation 1995;91:2642–2654.
38. Lovelock JD, Monasky MM, Jeong E-M, Lardin HA, Liu H, Patel BG, Taglieri DM, Gu L, Kumar P, Pokhrel N, Zeng D, Belardinelli L, Sorescu D, Solaro RJ, Dudley SC. Ranolazine improves cardiac diastolic dysfunction through modulation of myofilament calcium sensitivity. Circ Res 2012;110:841–850.
39. Clarke CL, Grunwald GK, Allen LA, Barón AE, Peterson PN, Brand DW, Magid DJ, Masoudi FA. Natural history of left ventricular ejection fraction in patients with heart failure. Circ Cardiovasc Qual Outcomes 2013;6:680–686.
40. Hwang SJ, Melenovsky V, Borlaug BA. Implications of coronary artery disease in heart failure with preserved ejection fraction. J Am Coll Cardiol 2014;63:2817–2827.
41. Dunlay SM, Roger VL, Weston SA, Jiang R, Redfield MM. Longitudinal Changes in Ejection Fraction in Heart Failure Patients With Preserved and Reduced Ejection Fraction. Circ Hear Fail 2012;5:720–726.
42. Heerebeek L van, Hamdani N, Falcão-Pires I, Leite-Moreira AF, Begieneman MP, Bronzwaer JG, Velden J van der, Stienen GJ, Laarman GJ, Somsen A, Verheugt FW, Niessen HW, Paulus WJ. Increased nitrosative/oxidative stress lowers myocardial protein kinase G activity in heart failure with preserved ejection fraction. BMC Pharmacol Toxicol BioMed Central; 2013;14:O2.
43. Franssen C, Chen S, Hamdani N, Paulus WJ. From comorbidities to heart failure with preserved ejection fraction: a story of oxidative stress. Heart 2016;102:320–330.
44. Bishu K, Hamdani N, Mohammed SF, Kruger M, Ohtani T, Ogut O, Brozovich F V, Burnett JC, Linke WA, Redfield MM. Sildenafil and B-type natriuretic peptide acutely phosphorylate titin and improve diastolic distensibility in vivo. Circulation 2011;124:2882–2891.
45. Krüger M, Kötter S, Grützner A, Lang P, Andresen C, Redfield MM, Butt E, Remedios CG dos, Linke WA. Protein kinase G modulates human myocardial passive stiffness by phosphorylation of the titin springs. Circ Res 2009;104:87–94.
46. Bull M, Methawasin M, Strom J, Nair P, Hutchinson K, Granzier H. Alternative Splicing of Titin Restores Diastolic Function in an HFpEF-Like Genetic Murine Model (TtnΔIAjxn). Circ Res American Heart Association, Inc.; 2016;119:764–772.
47. Weinberg EO, Shimpo M, Keulenaer GW De, MacGillivray C, Tominaga S, Solomon SD, Rouleau J-L, Lee RT. Expression and regulation of ST2, an interleukin-1 receptor family member, in cardiomyocytes and myocardial infarction. Circulation American Heart Association, Inc.; 2002;106:2961–2966.
48. AbouEzzeddine OF, McKie PM, Dunlay SM, Stevens SR, Felker GM, Borlaug BA, Chen HH, Tracy RP, Braunwald E, Redfield MM. Suppression of Tumorigenicity 2 in Heart Failure With Preserved Ejection Fraction. J Am Heart Assoc American Heart Association, Inc.; 2017;6:e004382.
49. Dieplinger B, Mueller T. Soluble ST2 in heart failure. Clin Chim Acta Elsevier; 2015;443:57–70.

Supplementary Materials

Supplementary Figures

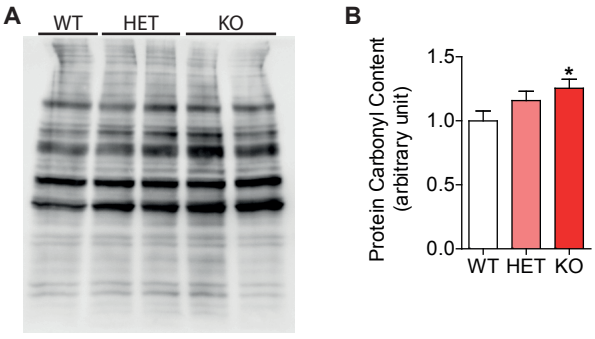

Fig. S1. Oplah knock-out mice have more left ventricular protein oxidation.
A. Representative immunoblot analysis of DNP (2,4 dinitophenyl hydrazine) derivatized oxidized proteins (total protein carbonyl content) in the left ventricles of Oplah knock-out (KO), heterozygous (HET), and wild-type littermates (WT). **B.** Quantified levels of the total protein carbonyl content in the KO (n =7), HET (n = 8) and WT (n = 6) mice. Levels were calculated as fold-change relative to WT levels. Data are presented as means ± SEM *, P < 0.05, as calculated Student's T-test.

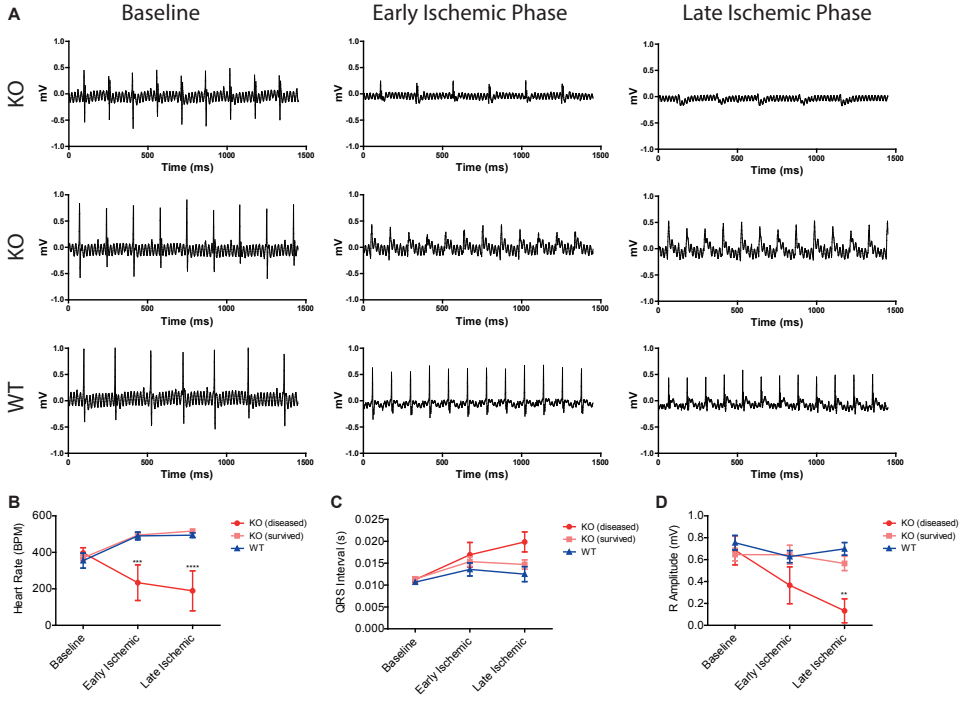

Fig. S2. Oplah knock-out mice are more prone to sudden death following ischemic injury.
A. Representative electrocardiography (ECG) images of Oplah knock-out (KO) and wild-type littermates (WT) at baseline, within the first 15 min following ischemic injury (early ischemic phase), and in the final 15 min following ischemic injury (late ischemic phase). (**TOP**) ECG of KO mice that exhibited sudden death. (**MIDDLE**) ECG of KO mice that survived ischemic injury. (**BOTTOM**) ECG of WT mice. **B-D.** ECG analysis of heart rate (**B**), QRS interval (**C**) and R amplitude (**D**) of the KO animals that died during the procedure (n = 4), KO animals that survived the procedure (n = 14), and WT mice (n = 5). Data are presented as means ± SEM **, P < 0.01; ***, P < 0.001; ****, P < 0.0001 as calculated by two-way analysis of variance (ANOVA).

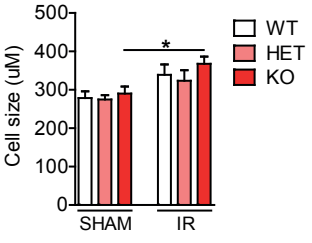

Fig. S3. Oplah KO mice have increased left ventricular hypertrophy post cardiac ischemia/reperfusion (IR) injury.
Quantified cell size of the WGA stained slices from the IR study (WT sham n = 12, WT IR n = 5, KO sham n = 11, KO IR n = 5). Data are presented as means ± SEM *, P < 0.05, as calculated Student's T-test.

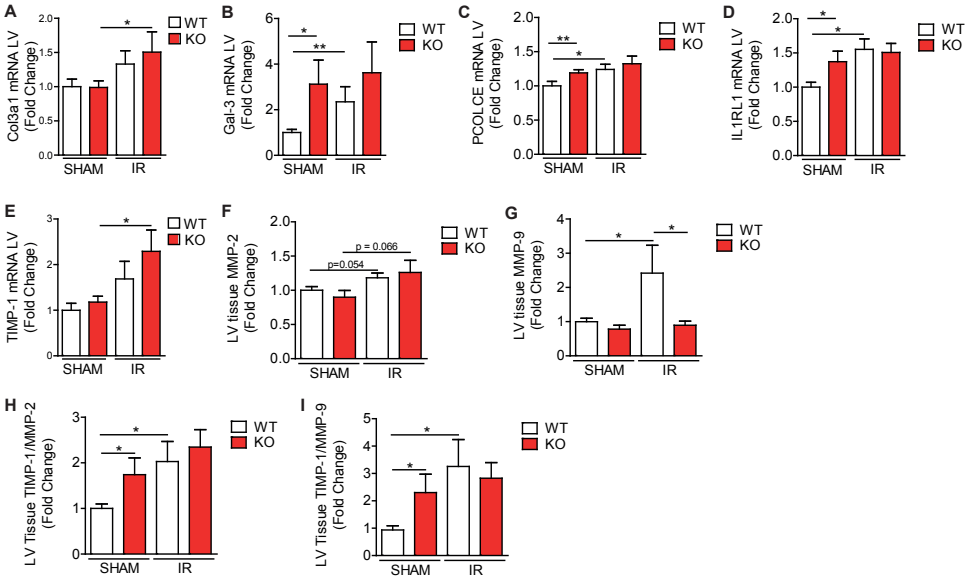

Fig. S4. Oplah knock-out mice have more cardiac fibrosis following cardiac ischemia/reperfusion (IR) injury.
A-G. qRT-PCR analysis of LV mRNA (WT SHAM n = 15, WT IR n = 11, KO SHAM n = 14, KO IR n = 10), for (**A**) Collagen type 3, alpha 1 (*Col3a1*), (**B**) Galectin-3 (*Gal-3*), (**C**) Procollagen C-endopeptidase enhancer 1 (*Pcolce*), (**D**) Interleukin 1 receptor-like 1 (*Il1rl1*, also known as *St2*), (**E**) TIMP metallopeptidase inhibitor 1 (*Timp-1*), (**F**) matrix metallopeptidase 2 (*Mmp-2*), and (**G**) matrix metallopeptidase 9 (*Mmp-9*). **H-I.** The ratio between *Timp-1* and *Mmp-2* (**H**) and *Mmp-9* (**I**). Data are presented as means ± SEM *, P < 0.05; **, P < 0.01 as calculated by one-way analysis of variance (ANOVA).

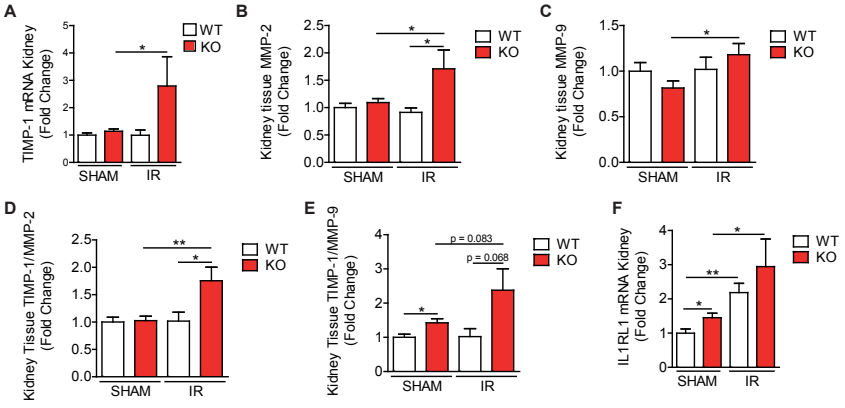

Fig. S5. Oplah knock-out mice have more renal fibrosis following cardiac ischemia/reperfusion (IR) injury.
A-C. qRT-PCR analysis of kidney mRNA (WT SHAM n = 10, WT IR n = 9, KO SHAM n = 15, KO IR n = 10), for (**A**) TIMP metallopeptidase inhibitor 1 (*Timp-1*), (**B**) matrix metallopeptidase 2 (*Mmp-2*), and (**C**) matrix metallopeptidase 9 (*Mmp-9*). **D-E.** The ratio between *Timp-1* and *Mmp-2* (**D**) and *Mmp-9* (**E**). **F.** qRT-PCR analysis of kidney mRNA for Interleukin 1 receptor-like 1 (*Il1rl1*, also known as *St2*). Data are presented as means ± SEM *, P < 0.05; **, P < 0.01 as calculated by one-way analysis of variance (ANOVA).

Supplementary Tables

Table S1. Primer sequences used in this study.

Transcript	Forward primer (5' - 3')	Reverse primer (5' - 3')
OPLAH (mouse/rat)	TCCGAGAGCTGGTCTTTC	ATTCACTGTGCGCCCATC
Timp-1 (mouse)	CTGCTCAGCAAGAGCTTTC	CTCCAGTTTGCAAGGGATAG
Mmp-2 (mouse)	CCCTGATGTCCAGCAAGTAG	GGAGTCTGCGATGAGCTTAG
Mmp-9 (mouse)	TCCCAGACGTGGGTCGATTC	GTCTCGCGGCAAGTCTTCAG
Col1a1 (mouse)	TTCTCCTGGCAAAGACGGAC	CCATCGGTCATGCTCTCTCC
Col3a1 (mouse)	GCGATTCAAGGCTGAAG	GGGTGCGATATCTATGATGG
ANP (mouse)	ATGGGCTCCTTCTCCATCAC	TCTACCGGCATCTTCTCCTC
α-MHC (mouse)	GTTAACCAGAGTTTGAGTGACA	CCTTCTCTGACTTTCGGAGGTACT
β-*MHC* (mouse)	ATGTGCCGGACCTTGGAAG	CCTCGGGTTAGCTGAGAGATCA
Gal-3 (mouse)	TATCCTGCTGCTGGCCCTTATG	GTTTGCGTTGGGTTTCACTG
PCOLCE (mouse)	TCAGTCTCCTTGGTGTCTAC	CTGACCCATCAGCAGATAAC
sST2 (mouse)	GCCAGAGTTGTGACTCATAG	CCCGGAGTAACACCATTATC
Catalase (mouse)	TTTTGCCTACCCGGACACTC	GGGGTAATAGTTGGGGGCAC
36B4 (mouse)	AAGCGCGTCCTGGCATTGTC	GCAGCCGCAAATGCAGATGG

Table S2. List of antibodies used in this study

Antigen	Cat. No.	Supplier
OPLAH	sc-271807	Santa Cruz Biotechnology Inc.
α-tubulin	t5168	Sigma-Aldrich

Table S3. Clinical characteristics of healthy control patient population

Demographics	n = 6
Age (years)	61.3 ± 7.0
Female sex n (%)	3 (50%)
BMI	26.1 ± 3.6
Systolic BP (mmHg)	136.8 ± 16.9
Medical History	
History of hypertension	1 (17%)
History of hypercholesterolemia	0 (0%)
History of diabetes mellitus	0 (0%)
Laboratory values	
NT-proNP, pg/ml	55.00 (32.00, 63.00)

Table S4. Clinical characteristics of HFpEF patients by 5-oxoproline concentrations

	5-oxoproline (3.7 - 6.7 µM)	5-oxoproline (6.7 - 12.8 µM)	
Demographics	**n = 26**	**n = 25**	**P value**
Age (years)	74.3 (10.8)	74.3 (8.6)	0.99
Female sex n (%)	20 (77%)	16 (64%)	0.31
NYHA n (%)			
II	7 (27%)	4 (16%)	0.34
III	19 (73%)	21 (84%)	
BMI	31.0 (7.7)	27.4 (4.2)	0.044
Systolic BP (mmHg)	140.0 (15.5)	143.1 (10.8)	0.41
Diastolic BP (mmHg)	72.8 (8.1)	75.9 (6.9)	0.15
Heart rate (bmp)	69.7 (8.9)	72.5 (12.2)	0.35
Comoridities %			
History of myocardial infarction	1 (4%)	1 (4%)	0.98
History of hypertension	22 (85%)	24 (96%)	0.17
History of atrial fibrilation	16 (94%)	16 (89%)	0.58
History of hypercholesterolemia	13 (50%)	13 (52%)	0.89
History of diabetes mellitus	9 (35%)	8 (32%)	0.84
Laboratory values			
Creatinine, µmol/l	82.0 (63.0, 112.0)	94.0 (77.0, 122.0)	0.16
NT-proNP, pg/ml	989.0 (403.0, 1681.0)	1087.0 (747.0, 1945.0)	0.26

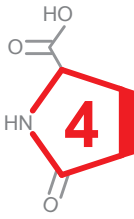

Table S5. Characteristics of Oplah KO mice compared to the clinical criteria for the diagnosis of HFpEF.

Clinical criteria for diagnosis of HFpEF	OPLAH KO mice
The presence of symptoms of HF	
Breathlessness, elevated jugular venous pressure, fatigue, etc.	N/A
A 'preserved' EF (LVEF ≥ 50%)	Preserved LVEF WT = 53.2 ± 2.6% HET = 55.3 ± 8.8% KO = 54.8 ± 2.9%
Elevated levels of NPs	Increased ANP expression (Fold change relative to WT) WT = 1.0 ± 0.3 HET = 1.6 ± 1.4 KO = 3.6 ± 2.2
Objective evidence of other cardaic functional and structural alterations underlying HF	
Left atrial volume index (LAVI) > 34 mL/m^2	Increased atria weight WT = 3.3 ± 0.4 mg/cm HET = 4.2 ± 0.8 mg/cm KO = 4.1 ± 0.3 mg/cm
Left ventricular mass index (LVMI) ≥ 115 g/m^2 (males) or ≥95 g/m^2 (females)	
Diastolic dysfunction	Impaired LV relaxation (Tau) WT = 6.8 ± 0.8 ms HET = 7.29 ± 1.0 ms KO = 8.5 ± 1.2 ms
Elevated LV filling pressures	
Pulmonary capillary wedge pressure (PCWP) ≥ 15 mmHg	
Left ventricular end diastolic pressure (LVEDP) ≥ 16 mmHg	Increased LVEDP WT = 5.8 ± 2.9 mmHg HET = 8.4 ± 4.2 mmHg KO = 11.3 ± 4.6 mmHg
Increased LV wall thickness	
Increased left atrial size	
Concomitant cardiovascular diseases (i.e. atrial fibrillation, hypertension, ect.)	
Concomitant non-cardiovascular diseases (i.e. kidney disease, diabetes, ect.)	Kidney damage/fibrosis WT = 1.7 ± 0.7% HET = 6.5 ± 3.1% KO = 5.0 ± 2.1%

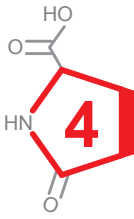
HO
O
HN
4
O